Neurobiology of Disease

The ducky^{2J} Mutation in *Cacna2d2* Results in Reduced Spontaneous Purkinje Cell Activity and Altered Gene Expression

Roberta Donato,[2]* Karen M. Page,[1]* Dietlind Koch,[1] Manuela Nieto-Rostro,[1] Isabelle Foucault,[1] Anthony Davies,[1] Tonia Wilkinson,[3] Michele Rees,[3] Frances A. Edwards,[2] and Annette C. Dolphin[1]

Departments of [1]Pharmacology and [2]Physiology, University College London, and [3]Department of Paediatrics and Child Health, Royal Free and University College Medical School, London WC1E 6BT, United Kingdom

The mouse mutant ducky and its allele ducky^{2J} represent a model for absence epilepsy characterized by spike-wave seizures and cerebellar ataxia. These mice have mutations in *Cacna2d2*, which encodes the $\alpha_2\delta$-2 calcium channel subunit. Of relevance to the ataxic phenotype, $\alpha_2\delta$-2 mRNA is strongly expressed in cerebellar Purkinje cells (PCs). The *Cacna2d2^{du2J}* mutation results in a 2 bp deletion in the coding region and a complete loss of $\alpha_2\delta$-2 protein. Here we show that *du^{2J}/du^{2J}* mice have a 30% reduction in somatic calcium current and a marked fall in the spontaneous PC firing rate at 22°C, accompanied by a decrease in firing regularity, which is not affected by blocking synaptic input to PCs. At 34°C, *du^{2J}/du^{2J}* PCs show no spontaneous intrinsic activity. *Du^{2J}/du^{2J}* mice also have alterations in the cerebellar expression of several genes related to PC function. At postnatal day 21, there is an elevation of tyrosine hydroxylase mRNA and a reduction in tenascin-C gene expression. Although *du^{2J}*/+ mice have a marked reduction in $\alpha_2\delta$-2 protein, they show no fall in PC somatic calcium currents or increase in cerebellar tryrosine hydroxylase gene expression. However, *du^{2J}*/+ PCs do exhibit a significant reduction in firing rate, correlating with the reduction in $\alpha_2\delta$-2. A hypothesis for future study is that effects on gene expression occur as a result of a reduction in somatic calcium currents, whereas effects on PC firing occur as a long-term result of loss of $\alpha_2\delta$-2 and/or a reduction in calcium currents and calcium-dependent processes in regions other than the soma.

Key words: **calcium channel; mouse mutant; $\alpha_2\delta$ subunit; mutation; spontaneous firing; Purkinje cell**

Introduction

A number of spontaneous autosomal recessive mouse strains have now been identified involving mutations in each of the subunits (α_1, β, and $\alpha_2\delta$) that together compose a voltage-gated calcium channel. They all have a similar phenotype that includes cerebellar ataxia and spike-wave seizures. Tottering (*Cacna1a^{tg}*, *tg/tg*) has a point mutation in $Ca_V2.1$ (α_1A) (Fletcher et al., 1996), and a number of alleles of this mutant have now been identified, as summarized recently (Zwingman et al., 2001). Lethargic (*Cacnb4^{lh}*) represents a truncation mutation of the β4 subunit (Burgess et al., 1997). Finally, two ducky alleles (*Cacna2d2^{du}*, *Cacna2d2^{du2J}*) both predict truncation mutations in the $\alpha_2\delta$-2 subunit (Snell, 1955; Barclay et al., 2001; Brodbeck et al., 2002), whereas the third ducky allele (*Cacna2d2^{entla}*) predicts a full-length protein with an inserted region in the α_2 moiety of $\alpha_2\delta$-2 (Brill et al., 2004). The original ducky allele (*du*) involves a gene duplication and inversion that disrupts the *Cacna2d2* gene within intron 3 but potentially also involves duplication and increased expression of other genes (Barclay et al., 2001).

The $\alpha_2\delta$-2 protein is strongly expressed in Purkinje cells (PCs) in the cerebellum (Barclay et al., 2001), and the cerebellum is reduced in size in *du/du* mice (Meier, 1968). However, although we found no loss of PC bodies at postnatal day 21 (P21), there was persistence of PCs with an immature or abnormal morphology in *du/du* cerebellum (Brodbeck et al., 2002). Furthermore, there was a reduction in calcium channel current in *du/du* PC somata at P7–P9 (Barclay et al., 2001). This was associated with loss of full-length $\alpha_2\delta$-2 protein and expression of a truncated mutant $\alpha_2\delta$-2 protein with aberrant function (Brodbeck et al., 2002).

The present study was undertaken to examine the basis for the ataxic phenotype in ducky mice. Rather than continuing with the original *du/du* allele, we have used mice carrying the *Cacna2d2^{du2J}* mutation. This represents a 2 bp deletion in exon 9 of *Cacna2d2* and is thus a simpler mutation than the complex rearrangement of the *Cacna2d2* gene, and the duplication of other genes, identified in the original *du/du* mice (Barclay et al., 2001). It is therefore likely to represent a clean knock-out of $\alpha_2\delta$-2 expression, allowing for easier interpretation of the mechanism involved in any changes observed. We found a reduction in

Received July 20, 2006; revised Oct. 23, 2006; accepted Oct. 25, 2006.

This work was supported by the Biotechnology and Biological Sciences Research Council , the Medical Research Council (United Kingdom), and the Wellcome Trust. We thank Stuart Martin for genotyping, Prof. V. H. Perry (Southampton University, Southampton, UK) for additional immunohistochemical experiments, Drs. Paola Pedarzani and Martin Stocker for discussion of results and reading this manuscript, and Mick Keegan for excellent technical assistance.

*R.D. and K.M.P. contributed equally to this work.

Correspondence should be addressed to Dr. Annette C. Dolphin, Laboratory of Cellular and Molecular Neuroscience, Andrew Huxley Building, Department of Pharmacology, University College London, Gower Street, London WC1E 6BT, UK. E-mail: a.dolphin@ucl.ac.uk.

DOI:10.1523/JNEUROSCI.3080-06.2006

calcium currents in PC somata and a decrease in the firing rate of intact PCs in cerebellar slices from homozygous mutant (du^{2J}/du^{2J}) compared with wild-type (WT; +/+) mice. Indeed, in the absence of synaptic input and at 34°C, the du^{2J}/du^{2J} PCs showed no spontaneous firing. Furthermore, we have identified alterations in the expression of specific genes relating to PC function in du^{2J}/du^{2J} cerebellum. Together, these results shed light on the mechanism of the ataxic phenotype exhibited by the du^{2J}/du^{2J} mice.

Materials and Methods

Genotyping. The $du^{2J}/+$ mice were obtained from The Jackson Laboratory (Bar Harbor, ME) and used to establish a colony. Genomic DNA was prepared from tail biopsies, and genotyping was performed with primers 5′-GGACGTCTTCATCAGCTTCA-3′ and 5′-6FAM-TATACAGGGG-GCCTCATCAC-3′, which produced a 219 bp product from the du^{2J} allele and a 221 bp product from the WT allele. Differences in product size were resolved on an Applied Biosystems (Foster City, CA) 373A DNA Sequencer running GeneScan 3.1.2 software. During the course of these studies, litters containing 113 +/+, 230 $du^{2J}/+$, and 121 du^{2J}/du^{2J} mice were genotyped, indicating that du^{2J}/du^{2J} shows no embryonic lethality.

RNA preparation for Affymetrix gene expression profiling. Three cerebella were pooled for each RNA extraction. Tissue was homogenized on ice using a ground glass homogenizer. The routine Trizol protocol was modified to deal with tissue of high lipid content. Isolated RNA was treated with DNase and purified through a Qiagen (Crawley, Sussex, UK) RNeasy column. RNA quality was checked on an Agilent (Palo Alto, CA) Bioanalyzer, and lack of genomic DNA contamination was confirmed by PCR.

Labeling and array hybridization. Sample labeling, hybridization, and scanning were performed as recommended by Affymetrix (Santa Clara, CA). A cDNA synthesis kit (Roche, Lewes, UK) was used, using 5 μg of total RNA. The cDNA was purified using Affymetrix cDNA cleanup columns, and *in vitro* transcription was performed using the ENZO Bio-Array HighYield RNA Transcript Labeling kit (Affymetrix), which results in biotinylated cRNA. Riboprobes were purified using Affymetrix cRNA columns, fragmented, and hybridized to the mouse expression arrays, MOE430A, which were then washed and stained following recommended Affymetrix protocols.

Scanning and data analysis. MOE430A arrays were scanned on the GeneChip Scanner 3000 and analyzed using Affymetrix GeneChip Operating software. Two separate sets of pooled samples were hybridized (totaling six animals per genotype) for each sibling-pair set comparison (+/+ vs du^{2J}/du^{2J} tissue), allowing a four-way comparison of data sets. After analysis, we first excluded all probe sets that showed no change in expression between the two arrays and those that were called as "absent" or "marginal" in both arrays. An arbitrary signal intensity cutoff value of 10 in both arrays was used to further exclude low-level expression probe sets. Genes were only chosen for additional investigation if their expression showed a ≥2-fold difference between one sibling-pair set comparison and at least a 1.4-fold difference in the other sibling-pair set.

Quantitative PCR. RNA was extracted from individual cerebella using the RNeasy lipid tissue kit and QiaShredders (Qiagen). Reverse transcription was performed on 1 μg of RNA using the iScript kit (Bio-Rad, Hercules, CA). Samples were diluted 1:10, and quantitative PCR (qPCR) was performed on an iCycler (Bio-Rad) using the iQ SYBR supermix. For each set of primers and for every experiment, a standard curve was generated using a serial dilution of reverse-transcribed RNA combined from different samples. Data were normalized for expression of both β-actin and the ribosomal protein L7a (RPL7a). For a list of primers used, see supplemental Table 1 (available at www.jneurosci.org as supplemental material).

Immunohistochemistry. All procedures conformed with the United Kingdom Animals (Scientific Procedures) Act of 1986. Mice, aged P21, were killed with CO_2 inhalation, and the cerebellum was dissected and fixed by immersion in ice-cold 4% paraformaldehyde. Fixed tissue was subject to a sucrose gradient for cryoprotection before sectioning. For immunohistochemistry, 40 μm sections were incubated overnight with rabbit anti-calbindin D-28K (1.46 μg/ml) at 4°C and detected with Texas Red-conjugated goat anti-rabbit antibody (Ab) (4 μg/ml; Invitrogen, Eugene, OR). In some experiments, the nuclear dye 4′,6-diamidino-2-phenylindole (500 nM; Invitrogen) was also used to visualize nuclei. Sections were viewed, and images were acquired with a Zeiss (Welwyn, UK) LSM confocal microscope.

Preparation of cerebellar tissue homogenates and Cos7 cell membranes. Cerebella, stored at −80°C, were thawed in ice-cold homogenization buffer [10 mM HEPES, pH 7.4, 150 mM NaCl, 300 mM sucrose, 2 mM EDTA, and protease inhibitors (Complete EDTA-free, 1 tablet/50 ml buffer; Roche)]. The tissue was homogenized using a hand-held Teflon/glass homogenizer, and cells were lysed by 10 passages through a 23 gauge needle, followed by three 5 s rounds of sonication. The lysed homogenate was centrifuged (12,000 × *g*, 10 min, 4°C), and the resultant supernatant was used in subsequent experiments. PBS-washed Cos7 cell pellets were resuspended in 25 vol of ice-cold lysis buffer [10 mM HEPES, pH 7.4, and protease inhibitors (Complete, used as above; Roche)] and lysed as above. Cell debris was removed by centrifugation (1000 × *g*, 15 min, 4°C), and the resultant supernatants were recentrifuged (100,000 × *g*, 60 min, 4°C) to pellet membranes. Protein concentrations in all preparations were determined by BCA assay (Perbio, Tatenhall, Cheshire, UK).

Immunoblotting. Immunoblot analysis was performed essentially as described previously (Page et al., 2004). Total protein (30 or 50 μg) was resolved by 3–8% SDS-PAGE, transferred to polyvinylidene difluoride membranes, and probed with relevant primary Abs and the appropriate horseradish peroxidase-conjugated secondary Abs, followed by enhanced chemiluminescence detection. Akt was detected as a loading control, and data were only compared when Akt loading was not different between samples. Data were quantified using ImageQuant 5.2, after verification that images were not saturated.

Primary Abs. The Abs used were $\alpha_2\delta$-2 rabbit polyclonal [anti-α_2-2(102–117)] (Brodbeck et al., 2002), anti-tenascin-C (MTn-12; Sigma-Aldrich, St. Louis, MO), anti-Akt (New England Biolabs, Beverly, MA), and anti-calbindin 48K (Chemicon, Temecula, CA).

PC preparation and dissociated cell electrophysiology. Calcium channel current recording from isolated PCs was performed as described previously (Barclay et al., 2001), except for the following points: cerebellar slices (300 μm) were prepared from P7–P11 mice using a vibrating tissue slicer and kept in 95%O_2/5% CO_2-saturated Krebs' solution for 30 min at 36°C before being cooled to room temperature. Cells were isolated immediately before use by digestion of slices with papain (20 U/ml) for 5–15 min, washed and triturated in Ringer's solution, and plated onto poly-L-lysine-coated coverslips. Ba^{2+} currents (I_{Ba}) were investigated by whole-cell patch-clamp recording. The internal (pipette) and external solutions and recording techniques were similar to those described previously (Campbell et al., 1995). The patch pipette solution contained the following (in mM): 140 Cs-aspartate, 5 EGTA, 2 $MgCl_2$, 0.1 $CaCl_2$, 2 K_2ATP, and 10 HEPES, pH 7.2, 310 mOsm, with sucrose. The external solution for recording Ba^{2+} currents contained the following (in mM): 150 tetraethylammonium (TEA) Br, 3 KCl, 1.0 $NaHCO_3$, 1.0 $MgCl_2$, 10 HEPES, 4 glucose, and 5 $BaCl_2$, pH 7.4, 320 mOsm, with sucrose. Pipettes of resistance 2–4 MΩ were used. An Axopatch 1D amplifier (Molecular Devices, Union City, CA) was used for recording, and data were filtered at 1–2 kHz and digitized at 5–10 kHz. Analysis was performed using Pclamp7 (Molecular Devices) and Origin 7 (Microcal Origin, Northampton, MA). Current records are shown after leak and residual capacitance current subtraction (P/4 protocol). The current density–voltage (*I–V*) relationships were fitted with a modified Boltzmann equation as follows:

$I = G_{max} \times (V - V_{rev})/(1 + \exp(-(V - V_{50,act})/k))$, where I is the current density (in picoamperes per picofarad), G_{max} is the maximum conductance (in nanosiemens per picofarad), V_{rev} is the reversal potential, $V_{50,act}$ is the midpoint voltage for current activation, and k is a slope factor.

PC recordings in cerebellar slices. Sagittal slices (300 μm thick) obtained from the cerebellum of P17–P25 mice (mean age, 19.7 ± 0.3) were prepared and maintained in artificial CSF containing the following (in mM): 125 NaCl, 2.4 KCl, 2 $CaCl_2$, 1 $MgCl_2$, 26 $NaHCO_3$, 1.1 NaH_2PO_4, and 25 glucose, saturated with 95% O_2/5% CO_2, pH 7.4. Cell-attached patch extracellular recordings in the voltage-clamp mode were obtained from PC somata under visual control for at least 10 min, before establishing the whole-cell configuration and switching into the current-clamp mode, using an Axopatch 1D patch-clamp amplifier. Patch pipettes were pulled from thick-walled borosilicate glass (World Precision Instruments, Hertfordshire, UK) to a tip resistance of 4–6 MΩ, when filled with an intracellular solution containing the following (in mM): 130 K-gluconate, 10 NaCl, 10 HEPES, 1 EGTA, 2 MgATP, and 1 $MgCl_2$, pH 7.4, with NaOH and an osmolarity of 298 mOsm, with 25 glucose. Data were acquired at 10 kHz with Digidata 1200 (Molecular Devices) using the programs WinWCP and WinEDR (kindly supplied by Dr. J. Dempster, University of Strathclyde, Glasgow, UK; available at https://spider.science.strath.ac.uk/spider/index.php). For the whole-cell current-clamp recordings, PCs were silenced by injecting a weak hyperpolarizing DC, to set the membrane potential to approximately −72 mV, before test pulses (10 pulses in 50 or 100 pA steps, 400 ms long) were applied. Membrane potentials were corrected off-line for the liquid junction potential, which was measured as −12 mV. Pclamp 9.0 (Molecular Devices) and GraphPad Prism 4.0 (GraphPad Software, San Diego, CA) were also used for data and statistical analysis. Analysis of firing rate was performed by using WinEDR software for detection of spontaneous events and the time course of the coefficient of variation (CV) for the instantaneous frequency (calculated as the reciprocal of the interevent interval) was calculated over a running average of 40 consecutive events.

The input resistance R_{in} was determined with brief −100 pA steps from −70 mV. The current threshold ($I_{threshold}$) for action potential firing was defined as the amount of injected current required to trigger a single action potential and was determined by incrementally increasing the amplitude of a current step in 50–100 pA increments from −70 mV. The potential threshold ($V_{threshold}$) for the first action potential was defined as the voltage at which dV/dt exceeded 25 mV/ms and was always confirmed by visual inspection of point of inflection at which the upstroke of the action potential occurs. PCs respond to hyperpolarizing current pulses with a depolarizing sag back to the holding potential (Williams et al., 2002), which is attributable to activation of the hyperpolarization-activated current (I_h). The amplitude of this sag was calculated by subtracting the steady-state potential (measured just before the offset of 400 ms negative current steps between 100 and 900 pA) from the peak potential. The criterion for inclusion of cells in any analysis was that in whole-cell mode they showed normal action potential firing to depolarizing current steps from a potential of −70 mV. Action potential firing could be induced in all cells that did not fire spontaneously in cell-attached mode.

For confocal imaging, the fluorescent dye Alexa Fluor-594 (absorption and emission maxima 588 and 613 nm, respectively; Invitrogen) was included in the intracellular solution (0.2 mg/ml) and allowed to diffuse for >15 min before imaging the neuron.

Data are given as mean ± SEM, and statistical significances between groups were determined by Student's unpaired *t* test, or by ANOVA followed by Tukey's multiple-comparison test, or using a nonparametric test, as appropriate.

The drugs used were as follows: ω-agatoxin-IVA and -IVB (Alomone Labs, Jerusalem, Israel), which were applied in bovine serum albumin (BSA; 25 μg/ml); penitrem A and apamin (Alomone Labs); SR95531 [2-(3-carboxypropyl)-3-amino-6-(4-methoxyphenyl)pyridazinium bromide], NBQX, and 7Cl-kynurenate (Tocris Bioscience, Bristol, UK); and TEA and nifedipine (Sigma, Poole, UK).

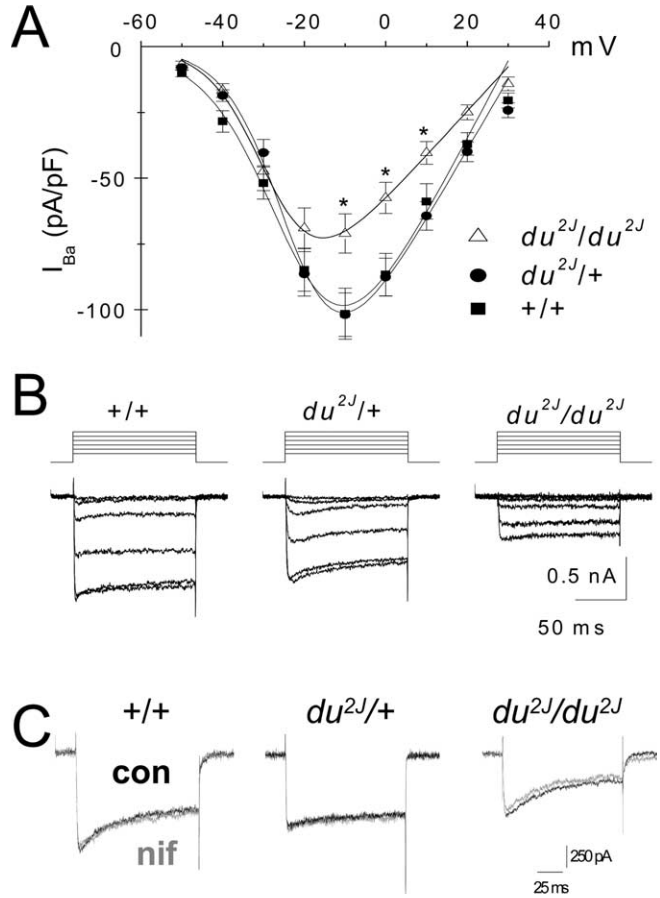

Figure 1. Whole-cell calcium channel currents in acutely dissociated PCs from du^{2J}/du^{2J}, $du^{2J}/+$, and +/+ cerebellum. ***A***, *I–V* relationships for whole-cell I_{Ba} in PCs from du^{2J}/du^{2J} (△; $n = 25$ cells, 9 mice), $du^{2J}/+$ (●; $n = 49$ cells, 19 mice), and +/+ (■; $n = 42$ cells, 11 mice). Data are mean ± SEM. *$p < 0.05$ at −10, 0, and +10 mV for du^{2J}/du^{2J} compared with +/+. ***B***, Representative examples of families of I_{Ba} from the three genotypes, from a holding potential of −80 mV to test potentials between −50 and 0 mV. ***C***, Representative examples of peak PC I_{Ba} at −10 mV, from the three genotypes, recorded before (black trace) and during (gray trace) application of 10 μM nifedipine (nif). The charge carrier was 5 mM Ba^{2+}. con, Control.

Results

The du^{2J} mutation results in a reduction in whole-cell calcium channel currents in acutely dissociated PC bodies

We have shown previously that I_{Ba} is reduced in isolated PC somata from *du/du* mice (Barclay et al., 2001). To test whether the same was true in du^{2J}/du^{2J} mice, I_{Ba} was examined in acutely dissociated cerebellar PCs from P7–P11 mice. The I_{Ba} density was significantly decreased in PCs from du^{2J}/du^{2J} compared with +/+ and $du^{2J}/+$ mice by ~30% (Fig. 1*A*,*B*; Table 1). In contrast, there was no reduction in calcium channel currents in heterozygous ($du^{2J}/+$) compared with WT PCs (Table 1). There was no significant effect on the voltage dependence of activation (Fig. 1*A*, Table 1), or on the kinetics of activation (data not shown), or on the rate of inactivation (Table 1). Cell size, as determined by the capacitance, was not significantly different between the genotypes (Table 1).

The PC calcium channel currents showed the expected pharmacology, being sensitive to ω-agatoxin-IVA (data not shown). Furthermore, there was no compensatory increase in L-type calcium channel current in the du^{2J}/du^{2J} PC somata, because the percentage of current blocked by 10 μM nifedipine was very small (<5%) in all three genotypes (Fig. 1*C*, Table 1). Calcium channel currents in PCs from older ages than P11 could not routinely be studied (as observed previously by many groups), because of problems of PC viability when dendrites are severed to form the isolated cell bodies required for voltage-clamping PCs. We did not observe a tendency toward an increased reduction in calcium currents in du^{2J}/du^{2J} PCs between P7 and P10, but this might have become apparent if it had been possible to record from PCs from older mice.

Table 1. Properties of WT, *du^{2J}/+*, and *du^{2J}/du^{2J}* PC calcium channel currents

	Genotypes		
	+/+	*du^{2J}/+*	*du^{2J}/du^{2J}*
Peak I_{Ba} at −10 mV (pA/pF)	−101.5 ± 9.7 (42)	−101.8 ± 8.2 (49)	−71.0 ± 7.4 (25)*
G_{max} (nS/pF)	3.1 ± 0.3 (42)	2.9 ± 0.2 (49)	1.9 ± 0.2 (25)**
Capacitance (pF)	20.6 ± 2.1 (42)	19.3 ± 1.4 (49)	22.5 ± 1.7 (25)
$V_{50,act}$ (mV)	−21.7 ± 1.3 (42)	−21.6 ± 1.0 (49)	−26.5 ± 1.8 (25)
$I_{(plateau)}/I_{(peak)}$ at −10 mV	0.64 ± 0.02 (29)	0.70 ± 0.02 (49)	0.69 ± 0.04 (22)
% Inhibition by 10 μM nifedipine	5.0 ± 5.0 (12)	0.0 ± 4.0 (11)	0.0 ± 2.0 (4)

Individual *I–V* relationships were fit by a modified Boltzmann function, and the $V_{50,act}$ and G_{max} were determined from this. $I_{plateau}/I_{peak}$ was determined from 100 ms steps; $I_{plateau}$ was measured just before repolarization. Statistical significances of the difference between *du^{2J}/du^{2J}* and WT are indicated by $*p < 0.05$ and $**p < 0.001$ (Student's *t* test). The numbers in parentheses indicate number of cells.

Comparison of spontaneous and evoked PC firing in slices from *du^{2J}/du^{2J}* and WT cerebellum

The inhibitory PCs are the only output neuron of the cerebellar cortex and thus, although many factors contribute to their activity, finally the firing pattern of PCs is the sole variable that determines the role of the cerebellar cortex in influencing motor activity and other functions. Because one of the main phenotypes resulting from the *du* mutation is cerebellar ataxia, it was of interest to study the effect of the loss of the $\alpha_2\delta$-2 Ca^{2+} channel subunit on PC firing.

The firing pattern of developing PCs, as well as their morphology and dendritic organization, undergoes dramatic changes during the first 2 weeks after birth (Woodward et al., 1969; Crepel, 1971; Cingolani et al., 2002). After about P14, an increasing proportion of mouse cerebellar PCs fire spontaneously, even in the absence of synaptic input (Womack and Khodakhah, 2002). We could not routinely measure PC firing at the same age that the whole-cell I_{Ba} recordings were made (P7–P11), because very few cells fired spontaneously at that age. Hence, in the first instance, we examined the spontaneous firing patterns of PCs at P17–P25. Cerebellar PCs show increasingly complex firing patterns as they mature. Whereas tonic firing can be recorded in the absence of dendrites, the trimodal burst firing that is observed more frequently in mature PCs involves a contribution from dendritic conductances (Womack and Khodakhah, 2002). In this study, we have analyzed in detail the tonic-firing PCs, but similar results were found for burst-firing cells (data not shown).

When recordings were made at 22–24°C, a small proportion of PCs failed to fire spontaneously in all groups (2 of 9 +/+ compared with 5 of 21 *du^{2J}/+* and 4 of 17 *du^{2J}/du^{2J}*) (Fig. 2*A*). However, for the cells that fired tonically, the PCs from *du^{2J}/du^{2J}* cerebella fired at much lower rates (Fig. 2*B*,*C*) and also showed an increased irregularity of firing, as measured by the CV (Fig. 2*D*). Surprisingly, tonically firing PCs from *du^{2J}/+* mice showed a firing rate that was intermediate between WT and *du^{2J}/du^{2J}* PCs (Fig. 2*C*), although the firing frequency was as regular as that of WT PCs (Fig. 2*D*).

Changes in synaptic transmission, particularly GABAergic transmission, influence the rate and pattern of firing of PCs (Hausser and Clark, 1997). To investigate whether the lower PC firing frequency depended on a change of synaptic input, we blocked both glutamatergic and GABAergic synaptic currents by the addition of the $GABA_A$ antagonist SR95531 (6 μM), the AMPA/kainate receptor antagonist 7Cl-kynurenate (10 μM), and the NMDA receptor antagonist NBQX (20 μM). The presence of these blockers did not abolish the difference between the three genotypes. At 22°C, the spontaneous tonic firing frequency was 23.1 ± 3.7 Hz ($n = 3$) for +/+ compared with 15.3 ± 1.3 Hz ($n = 8$) for *du^{2J}/+* ($p < 0.05$ vs +/+) and 8.1 ± 1.5 Hz ($n = 4$) for *du^{2J}/du^{2J}* PCs ($p < 0.01$ vs +/+ and $p < 0.05$ vs *du^{2J}/+*). The regularity of firing, measured by the CV, was 0.11 ± 0.02 ($n = 3$)

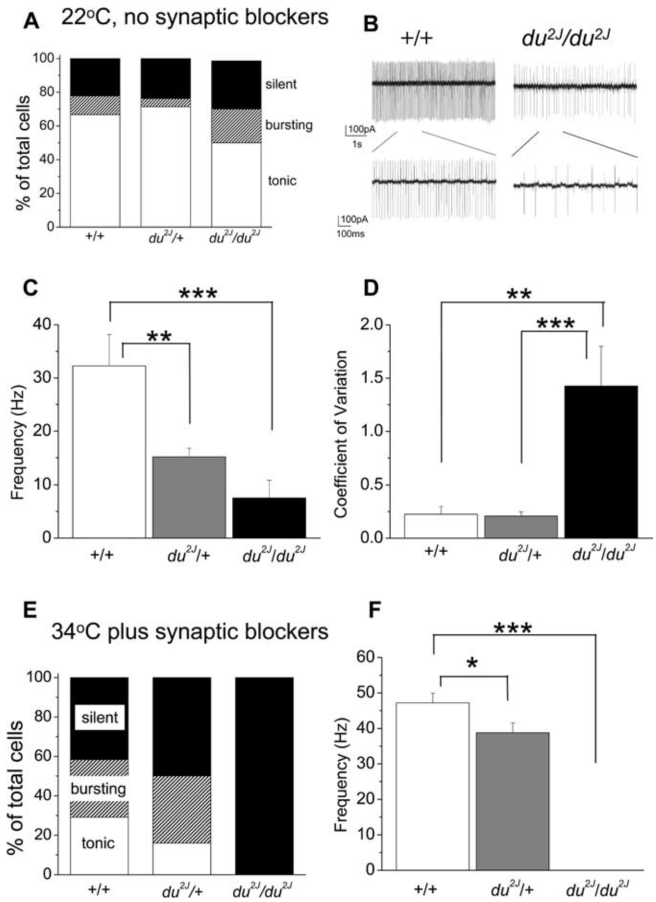

Figure 2. Spontaneous firing properties of cerebellar PCs from +/+, *du^{2J}/+*, and *du^{2J}/du^{2J}* mice. ***A***, Percentage of PCs that are silent (black bar) or firing either tonically (white bar) or in a bursting pattern (hatched bar), when recorded in cell-attached mode at 22°C and in the absence of any synaptic blockers, for +/+ ($n = 9$ cells from 3 mice), *du^{2J}/+* ($n = 21$ cells from 5 mice), and *du^{2J}/du^{2J}* ($n = 17$ cells from 6 mice). ***B***, Continuous recordings in cell-attached mode showing a typical example of tonic firing pattern of a +/+ cell (left) and a *du^{2J}/du^{2J}* cell (right) at room temperature and in the absence of synaptic blockers. The bottom panel shows the regions delineated on an expanded time scale. ***C***, Mean instantaneous tonic firing frequency for +/+ (white bar; $n = 6$ cells from 3 mice), *du^{2J}/+* (gray bar; $n = 14$ cells from 5 mice), and *du^{2J}/du^{2J}* (black bar; $n = 8$ cells from 6 mice). $***p < 0.001$ $**p < 0.01$ (ANOVA and Tukey's multiple-comparison test). ***D***, CV of firing rates for the tonically firing cells analyzed in ***C***. $***p < 0.001$, $**p < 0.01$ (ANOVA and Tukey's multiple-comparison test). ***E***, Percentage of PCs that are silent (black bar) or firing either tonically (white bar) or in a bursting pattern (hatched bar), when recorded in cell-attached mode at 34°C and in the presence of synaptic blockers (6 μM SR95531, 20 μM NBQX, 10 μM 7Cl-kynurenate), for +/+ ($n = 24$ cells from 5 mice, P19–25), *du^{2J}/+* ($n = 50$ cells from 9 mice, P17–24), and *du^{2J}/du^{2J}* ($n = 26$ cells from 5 mice, P19–22). ***F***, Mean instantaneous firing frequency for tonically firing PCs, for +/+ (white bar; $n = 7$), *du^{2J}/+* (gray bar; $n = 8$), and *du^{2J}/du^{2J}* (0 of 26; note that none of the *du^{2J}/du^{2J}* cells exhibited any spontaneous firing) recorded at 34°C in the presence of synaptic blockers. $*p < 0.05$, $***p < 0.001$ (ANOVA and Tukey's multiple-comparison test). Error bars indicate SEM.

for +/+ compared with 0.13 ± 0.02 (n = 8) for du^{2J}/+ and 2.71 ± 0.65 (n = 4) for du^{2J}/du^{2J} ($p < 0.01$ vs +/+ and du^{2J}/+) PCs. Hence, the difference in firing frequency between the genotypes was clearly not dependent on changes in GABA or glutamate release affecting the properties of the PCs.

It is well known that the spontaneous activity of PCs depends on the temperature (Womack and Khodakhah, 2002). To ensure that the effects we were studying were physiologically relevant, we repeated these experiments at close to physiological temperatures (33–34°C), again in the presence of the synaptic blockers. At the higher temperature, the most obvious difference observed was that no du^{2J}/du^{2J} PCs were observed to fire spontaneously when recorded in the cell-attached mode (n = 26 cells from five mice), whereas a similar proportion of +/+ and du^{2J}/+ PCs still fired spontaneously, although a larger percentage showed a bursting pattern of firing (Fig. 2E). The firing frequency of the tonically firing du^{2J}/+ PCs (n = 8) remained significantly lower than that of +/+ PCs, although to a smaller extent than at 22°C (n = 7) (Fig. 2F), whereas the regularity of firing remained similar (CV was 0.08 ± 0.01 for +/+ and 0.14 ± 0.02 for du^{2J}/+; $p > 0.05$), in agreement with the data obtained at 22°C. In all three conditions examined, there was no consistent correlation between tonic firing frequency and postnatal age, and the effect on firing frequency in du^{2J}/du^{2J} PCs was observed at all ages measured (data not shown).

For all cells, after cell-attached recording, whole-cell recordings were performed to measure passive and active membrane properties of the neurons and to confirm their viability. In whole-cell mode, at 34°C in the presence of synaptic blockers, the input resistance (R_{in}) was not significantly affected by the mutation (Fig. 3A). At 22°C, the R_{in} was higher but was also not significantly different between the two genotypes (data not shown). For +/+ PCs, the resting potential (V_{rest}) could not be determined accurately, because the cells fired spontaneously unless hyperpolarizing current was injected, whereas du^{2J}/du^{2J} PCs were silent at 34°C in the presence of synaptic blockers, both in cell-attached mode and in whole-cell mode, and their V_{rest} was −47.2 ± 1.1 mV (n = 30). This value is very similar to that determined for PCs in BK knock-out mice, which also show less spontaneous activity (Sausbier et al., 2004), a behavior attributed to depolarization block of Na_V channels. Consistent with this view of the mechanism for silencing, there is a transient resumption of spontaneous activity in otherwise silent du^{2J}/du^{2J} PCs after injection of hyperpolarizing current pulses to −72 mV (data not shown).

When the membrane potential was set to approximately −72 mV and depolarizing current steps were injected in current-clamp mode, it was possible to evoke action potentials in du^{2J}/du^{2J} as well as +/+ PCs (Fig. 3B). The pattern of firing in response to current injection was different, with considerably greater spike frequency accommodation occurring in du^{2J}/du^{2J} PCs (Fig. 3B). For 900 pA current injection, 18 of 28 (64%) of the +/+ PCs continued firing until the end of the 400 ms step, whereas only 7 of 30 (23%) of the du^{2J}/du^{2J} PCs showed the same behavior. The estimated membrane potential at which the first action potential was initiated ($V_{threshold}$) was very similar in +/+ and du^{2J}/du^{2J} PCs (Fig. 3C), and it is notable that in du^{2J}/du^{2J} PCs this was −49.5 ± 0.8 mV, not significantly different from V_{rest} in these cells. However, the minimum amount of depolarizing current required to induce firing ($I_{threshold}$) was markedly increased in du^{2J}/du^{2J} PCs (Fig. 3C).

For the first action potential evoked by $I_{threshold}$ from −72 mV, there was no significant difference in the half-width or in the rise time between +/+ and du^{2J}/du^{2J} PCs and no difference in the characteristics of the afterhyperpolarization after this action potential (data not shown). Furthermore, there was no effect on the sag attributable to I_h measured with 400 ms hyperpolarizing current steps of between 100 and 900 pA from −72 mV. In response to the −900 pA step, it was 12.5 ± 2.9 mV in +/+ PCs (n = 5) and 12.3 ± 2.3 mV in du^{2J}/du^{2J} PCs (n = 10).

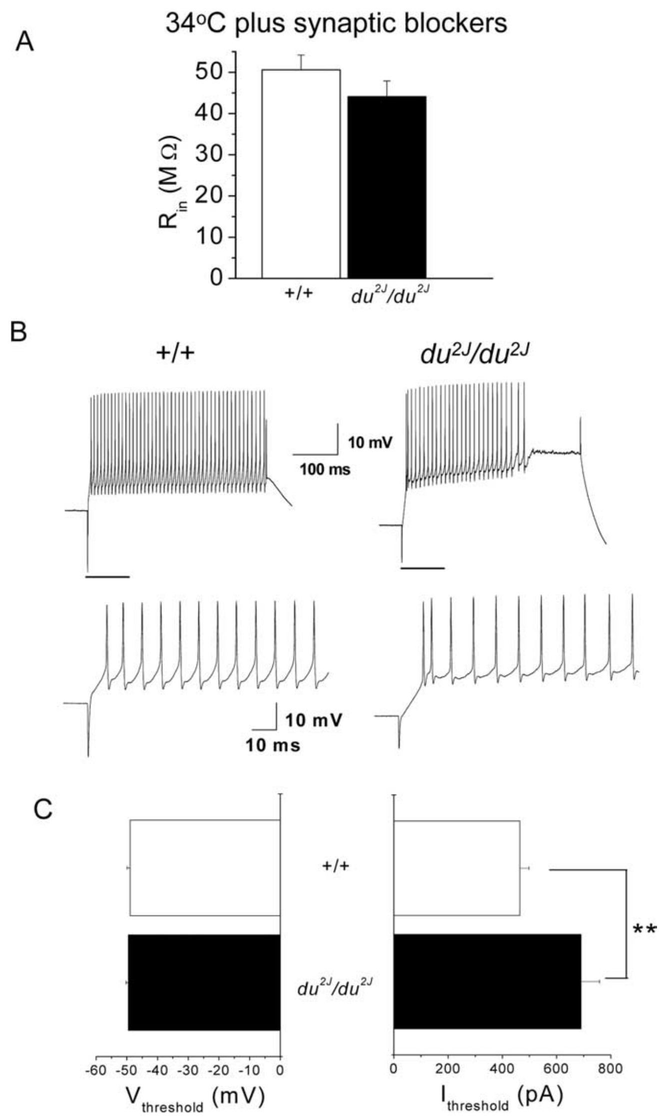

Figure 3. Properties of cerebellar PCs in whole-cell mode from +/+ and du^{2J}/du^{2J} mice. ***A***, Membrane input resistance (R_{in}) for +/+ (□; n = 28) and du^{2J}/du^{2J} (■; n = 30) measured at 34°C and in the presence of synaptic blockers. Values are not significantly different between the two genotypes (p = 0.19, Student's unpaired t test). ***B***, Example of voltage responses evoked in current clamp by injection of a 900 pA current step (400 ms duration). Recording conditions are as in ***A***, except cells were maintained at −72 mV before application of depolarizing current steps. Left, Typical response evoked in a +/+ cell. The firing is sustained until the end of the step, with little adaptation. Right, Characteristic response of a du^{2J}/du^{2J} PC. After the first few spikes, a plateau develops before the end of the stimulus. Note also that this PC did not fire spontaneously in cell-attached mode. The bottom panel shows expanded sections of the traces indicated by the horizontal bars in the top panel. ***C***, Estimate of $V_{threshold}$ (in millivolts; left) and $I_{threshold}$ (in picoamperes; right) required for the generation of the first action potential (determined as described in Materials and Methods), measured in responses evoked by depolarizing current steps (50–100 pA increments, 400 ms duration from a holding potential of approximately −72 mV) for +/+ (□; n = 28) and du^{2J}/du^{2J} (■; n = 30) PCs. Note that although the $V_{threshold}$ is not significantly different between the genotypes (p = 0.09), the $I_{threshold}$ is significantly higher for the du^{2J}/du^{2J} compared with +/+ PCs (** p = 0.01, Mann–Whitney U test).

To investigate the underlying cause of the differences between the firing properties of +/+ and *du*[2J]/*du*[2J] PCs, we also studied the effect of specific channel antagonists. The changes could be either directly attributable to the acute effect of the observed decrease in Ca^{2+} influx via voltage-gated calcium channels, or they could be indirect and attributable to longer-term changes in gene expression, affected by a reduction in Ca^{2+} influx during development. We thus inhibited Ca^{2+} influx through voltage-gated calcium channels in WT cerebellar slices to imitate the acute situation in *du*[2J]/*du*[2J] mice. Adding ω-agatoxin-IVB (100 nM; a selective blocker of P-type calcium channels) to the bath solution, while recording from spontaneously firing +/+ PCs in the cell-attached patch configuration, resulted in a brief period of increased firing frequency (Fig. 4*A*), followed by bursting (Fig. 4*A*). We found that the increase in firing frequency after blockade of P-type channels was always accompanied by a decrease in firing precision (Fig. 4*B*), rather than being preceded by the decrease in precision as reported previously (Walter et al., 2006). Subsequently, the spontaneous firing of action potentials was completely blocked (Fig. 4*A*,*C*). Similar behavior was observed in three other tonically firing +/+ PCs. For three additional cells that were initially burst firing under control conditions, ω-agatoxin-IVB also induced the total arrest of their spontaneous activity. These results are consistent with the observations of Womack and Khodakhah (2002), demonstrating that Ca^{2+} entry through P-type Ca^{2+} channels is required for spontaneous activity in PCs. However, a proviso to this conclusion is that the concentration of ω-agatoxin-IVB used here is likely to cause a more complete block of P-type currents than the modest reduction observed in isolated *du*[2J]/*du*[2J] PCs.

In the whole-cell configuration, it remained possible to evoke action potentials in +/+ PCs after application of ω-agatoxin-IVB, although the amount of current required to evoke action potential firing was increased, and there was increased spike frequency adaptation (Fig. 4*D*). For 900 pA current injection, zero of six PCs continued firing until the end of the 400 ms step in the presence of ω-agatoxin-IVB. Both of these effects were very similar to the behavior of *du*[2J]/*du*[2J] PCs. We thus concluded that the inhibition of spontaneous firing might be directly caused by reduction in inward Ca^{2+} flux, or to an imbalance between inward Ca^{2+} and outward K^+ conductances, resulting in a depolarization block. The latter possibility is suggested because it was still possible to evoke firing in silent cells after depolarization from a hyperpolarized membrane potential.

Although for technical reasons I_{Ba} measurements were performed on isolated PC somata at earlier ages than used in the slice experiments, unclamped Ba^{2+} currents were observed in both +/+ and *du*[2J]/*du*[2J] P15–P17 PCs in slices, after blockade of Na^+ and K^+ currents (data not shown).

To investigate the downstream cause of the reduction in PC firing frequency in *du*[2J]/*du*[2J] PCs, we examined the effect of the broad-spectrum K^+ channel blocker TEA and the selective Ca^{2+}-activated K^+ channel [$I_{K(Ca)}$] antagonists Penitrem A (to block BK channels) and apamin (to block SK channels). None of these compounds changed the WT firing pattern to that of *du*[2J]/*du*[2J] PCs. TEA (1 mM) caused a small but reversible increase in the firing rate of +/+ PCs (data not shown). In agreement with the published data on the role of $I_{K(Ca)}$ channels (Edgerton and Reinhart, 2003), blocking SK channels with apamin (100 nM) or blocking BK channels with Penitrem A (10 μM) also increased the rate of firing in +/+ PCs and resulted in a switch to burst firing (data not shown). It is therefore likely that the initial increase in firing rate seen in response to ω-agatoxin-IVB (Fig. 4*A*) may be

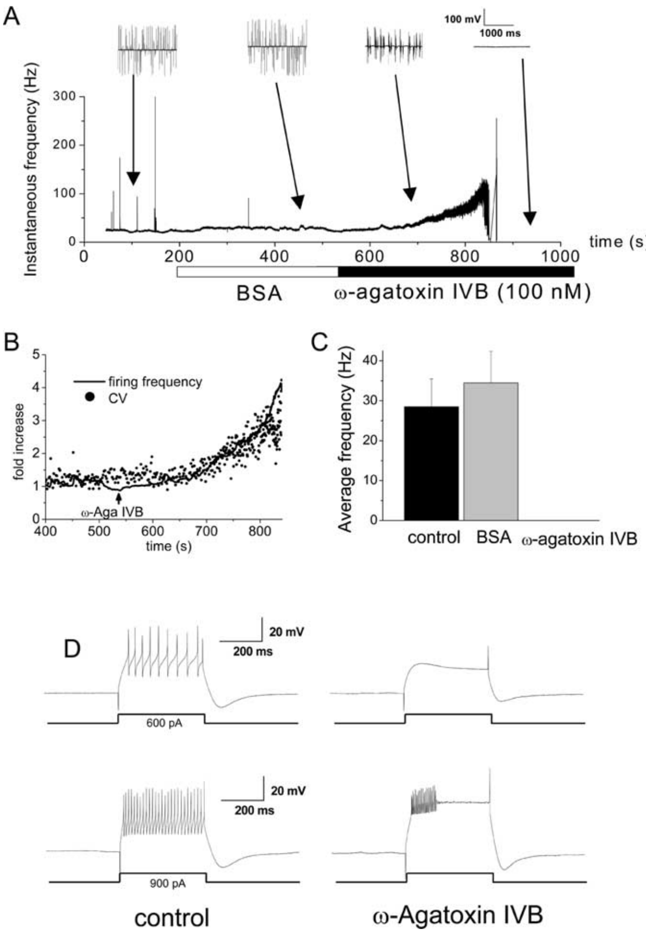

Figure 4. Effect of ω-agatoxin-IVB on spontaneous firing properties of cerebellar PCs from +/+ mice. ***A***, Example of the effect of ω-agatoxin-IVB on the time course of instantaneous spontaneous firing frequency of a +/+ PC, recorded in cell-attached mode at 34°C and with synaptic blockers in the control solution. The cell fires tonically in control. In the presence of BSA (25 μg/ml), the firing rate increases slightly for ~5 min. When ω-agatoxin-IVB (100 nM) is added to the superfusate, a dramatic increase in the frequency is initially observed, which develops into an irregular bursting firing pattern. The cell then enters a quiescent state for the rest of the recording in cell-attached mode (~5 min). Two-second blocks of data are shown above the graph for the periods indicated by the arrows. Similar data were obtained in three other cells that were initially firing tonically. ***B***, Expansion of part of Figure 4*A* to show the initial transient increase in firing frequency after ω-agatoxin-IVB application, plotted as fold increase (solid line). The simultaneous fold increase in the CV of the firing frequency is superimposed (filled circles). Similar data were obtained in three other cells that were initially firing tonically. ***C***, Average spontaneous firing frequency in control, BSA, and ω-agatoxin-IVB for +/+ PCs ($n = 6$). The slight increase in frequency in BSA is not statistically significant ($p = 0.1$, paired *t* test). ***D***, Firing evoked by a 600 pA (top traces) or a 900 pA (bottom traces) current pulse of 400 ms duration in control (left) and after >5 min in the presence of ω-agatoxin-IVB (right) in a +/+ PC. Under control conditions, the cell is able to fire action potentials throughout the duration of the 600 and 900 pA steps, whereas after ω-agatoxin-IVB, the 600 pA current is no longer sufficient to evoke firing (top right). In ω-agatoxin-IVB, the cell is still able to fire in response to a 900 pA current injection, although only with a few initial spikes accommodating to a plateau (bottom right), as typically seen in *du*[2J]/*du*[2J] PCs.

attributable to a decrease in the activation of $I_{K(Ca)}$, but the subsequent inhibition must be additionally caused by an effect on another conductance, such as Na^+ channel inactivation.

Changes in gene expression in *du*[2J]/*du*[2J] compared with WT cerebellum at different stages of development

To elucidate the role of the $\alpha_2\delta$-2 protein and whether the changes in PC firing related to changes in the expression of other genes, we performed microarray analysis, using Affymetrix GeneChips, on du^{2J}/du^{2J} and WT littermates. The gene showing the greatest degree of change in expression between WT and du^{2J}/du^{2J} cerebella was *Cacna2d2*, in which a reduction was observed across the entire age range studied. At P10 and P21, *Cacna2d2* was called as absent in the ducky samples; however, mRNA was present in the P0 samples. Because the du^{2J} mutation is a 2 bp deletion resulting in transcription of full-length mRNA but predicting a truncated protein, it is reasonable to expect some *Cacna2d2* mRNA to be detected in the samples, although the process of nonsense-mediated decay would be expected to result in the destruction of most of the mutant mRNA because it contains multiple nonsense codons (for review, see Maquat, 2002). These results imply that nonsense-mediated decay of *Cacna2d2* mRNA may be more effective in older animals. Furthermore, altered gene expression appears to change in du^{2J}/du^{2J} cerebellum over time. Other genes identified as having altered expression at P0 have no overlap with those identified at P21 (see supplemental Tables 2–4, available at www.jneurosci.org as supplemental material). This would imply that $\alpha_2\delta$-2 may have different functions at differing stages of development, or that anomalies in gene expression during the earlier stage may affect function and gene expression at the later stage. To corroborate this, no differences in gene expression (apart from *Cacna2d2*) were seen at P10 (supplemental Table 3, available at www.jneurosci.org as supplemental material).

In total, 23 genes on the MOE430A Affymetrix gene chip showed consistently altered expression in du^{2J}/du^{2J} mice at P21. Of these, 52% were downregulated and 48% were upregulated (supplemental Table 2, available at www.jneurosci.org as supplemental material). Major findings relate to the expression of two genes. First, mRNA for the extracellular matrix protein tenascin-C was downregulated by 1.7-fold in the Affymetrix arrays; this protein is synthesized by Bergmann glia in the cerebellum, which are mainly localized within the PC layer in adults (Yamada and Watanabe, 2002). Second, tyrosine hydroxylase mRNA was strongly upregulated, as also seen in a number of other cerebellar mutants. In addition, other transcripts that were downregulated included several genes that have a role in the circulatory system and angiogenesis, such as erythroid associated factor (*Eraf*), angiotensin receptor-like 1, solute carrier family 4 (*Slc4a1*), and lymphocyte antigen 68. Two others have been implicated in the glucocorticoid pathway (serum/glucocorticoid-regulated kinase and FK506-binding protein 5) (supplemental Table 2, available at www.jneurosci.org as supplemental material).

To test the reliability of the microarray results and to examine the alteration in expression of specific ion channels and splice variants of low abundance, we performed real-time qPCR, in particular at P21, on a separate set of samples from those used in the microarray analysis (Fig. 5 and supplemental Table 5, available at www.jneurosci.org as supplemental material). Data were normalized for the mean expression of β-actin and the ribosomal protein RPL7a, both of which were unchanged in du^{2J}/du^{2J} cerebellum (data not shown). Using this technique, tyrosine hydroxylase mRNA was found to be upregulated by 16.3 ± 0.79-fold ($n = 10$) in du^{2J}/du^{2J} cerebellum at P21 (Fig. 5*A*). In contrast, there was no change in cerebellar tyrosine hydroxylase gene expression in $du^{2J}/+$ cerebellum compared with WT cerebellum (Fig. 5*A*). Tyrosine hydroxylase gene expression was also unchanged in du^{2J}/du^{2J} mice at P0 (data not shown). Also in agreement with the microarray results, tenascin-C mRNA was reduced to $44 \pm 6\%$ ($n = 10$) in du^{2J}/du^{2J} cerebellum (Fig. 5*B*),

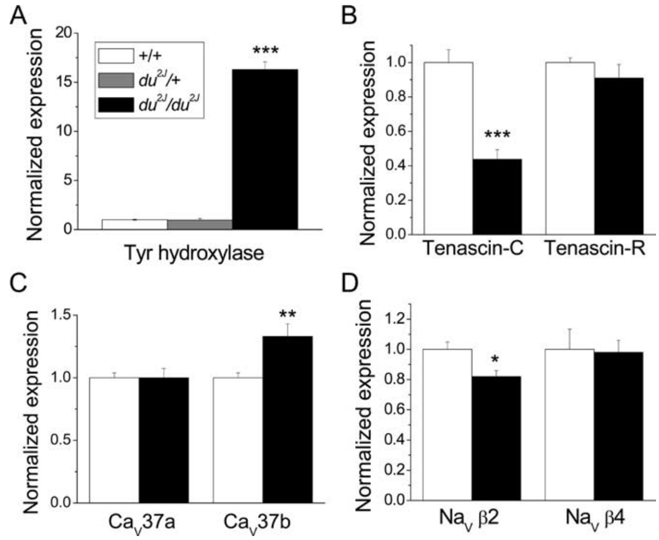

Figure 5. Comparison of gene expression in du^{2J}/du^{2J} and $+/+$ cerebellum at P21 by qPCR. RNA was isolated from the cerebellum of mice at developmental stage P21, and qPCR was performed as described in Materials and Methods. Expression was corrected for the mean expression of the housekeeping genes actin and RPL7a, neither of which was found altered in du^{2J}/du^{2J} mice, and normalized to expression in WT cerebellum. Data are from $+/+$ (white bars), $du^{2J}/+$ (where measured; gray bar), and du^{2J}/du^{2J} (black bars). ***A***, Tyrosine hydroxylase (Tyr hydroxylase) mRNA ($n = 15$ $+/+$; $n = 8$ $du^{2J}/+$; $n = 10$ du^{2J}/du^{2J}). ***B***, Tenascin-C mRNA ($n = 15$ $+/+$, $n = 10$ du^{2J}/du^{2J}) and tenascin-R mRNA ($n = 5$ for both genotypes). ***C***, Ca_V37a and Ca_V37b ($n = 15$ $+/+$, $n = 10$ du^{2J}/du^{2J}). ***D***, $Na_V\beta2$ ($n = 10$ for both genotypes) and $Na_V\beta4$ ($n = 5$ for both genotypes). The statistical significances of the changes observed in du^{2J}/du^{2J} compared with $+/+$ cerebellum are given by $^{***}p < 0.0001$, $^{**}p < 0.01$, and $^{*}p < 0.02$ (Student's *t* test). Full data are shown in supplemental Table 5 (available at www.jneurosci.org as supplemental material).

whereas expression of the related gene tenascin-R was unaffected (Fig. 5*B*).

Additional qPCR was performed on candidate ion channel gene expression that might be upregulated or downregulated, to shed further light on the reduction in PC firing observed in du^{2J}/du^{2J} cerebellar slices (described above). The expression of the calcium channel subunits $\alpha_2\delta$-1, $Ca_V\beta1$, $Ca_V\beta2$, $Ca_V\beta4$, $Ca_v1.2$, $Ca_v1.3$, $Ca_v2.2$, and $Ca_v3.1$ was not altered (supplemental Table 5, available at www.jneurosci.org as supplemental material). The splice variant of $Ca_V2.1$ containing exon 37a has been found to be upregulated during PC development and gives rise to larger currents that show calcium-dependent facilitation (Chaudhuri et al., 2004). We therefore examined whether the prevalence of exons 37a and 37b was altered in du^{2J}/du^{2J} mice and found that although the expression of $Ca_V2.1$ was not significantly increased when primers were used in a constitutive exon, the prevalence of exon 37b was increased by $32.7 \pm 10\%$ ($n = 10$) in du^{2J}/du^{2J} cerebellum (Fig. 5*C*). Using a number of different methods, we found that $Ca_V2.1$ channels containing exon 37a were expressed at approximately threefold higher levels than those containing exon 37b in both $+/+$ and du^{2J}/du^{2J} cerebellum (data not shown). These results point to an altered distribution of P-type channels between somatic and dendritic compartments in du^{2J}/du^{2J} PCs, because it has previously been shown that exon 37b-containing $Ca_V2.1$ channels show greater localization in dendrites (Chaudhuri et al., 2005).

Despite the fact that Ca^{2+}-activated K^+ channels are important for the regulation of spontaneous PC firing (Swensen and Bean, 2003), there was no upregulation or downregulation of the main species underlying $I_{K(Ca)}$ in PCs (SK2, BK1, or BKβ4) (sup-

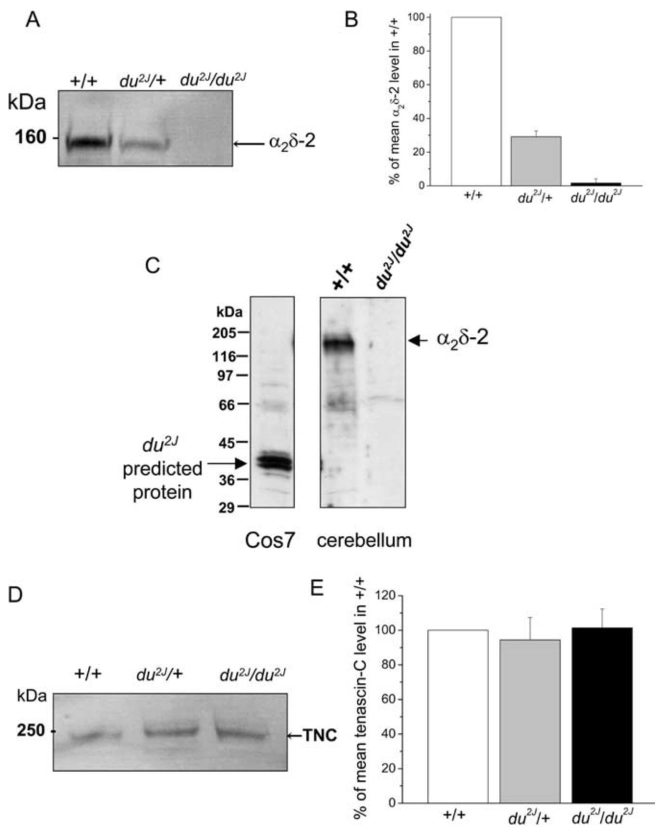

Figure 6. $\alpha_2\delta$-2 and tenascin-C protein expression in du^{2J}/du^{2J}, $du^{2J}/+$ and $+/+$ cerebellum at P21. ***A***, Representative immunoblots of cerebellar $\alpha_2\delta$-2 in $+/+$, $du^{2J}/+$, and du^{2J}/du^{2J} cerebellum. The Ab used in ***A*** and ***C*** was anti-α_2-2(102–117) anti-peptide Ab. ***B***, Quantification of cerebellar $\alpha_2\delta$-2 in $+/+$ (white bar), $du^{2J}/+$ (gray bar), and du^{2J}/du^{2J} (black bar) mice at P21 ($n = 5$). ***C***, Lack of evidence for the existence of a truncated protein product produced from the predicted mutant *Cacna2d2* transcript in du^{2J}/du^{2J} cerebellum. Left, Expression of a 40 kDa product formed from cDNA encoding the predicted sequence expressed in Cos7 cells. Right, Expression of native $\alpha_2\delta$-2 in $+/+$ and du^{2J}/du^{2J} cerebellum. Molecular weight markers are shown on the left. ***D***, Representative immunoblots of tenascin-C (TNC) protein expression in $+/+$, $du^{2J}/+$, and du^{2J}/du^{2J} cerebellum. At P21, only an ~250 kDa species was observed, whereas at younger ages an ~350 kDa band was the main immunoreactive species (data not shown). ***E***, Quantification of tenascin-C in cerebellum from $+/+$ (white bar), $du^{2J}/+$ (gray bar), and du^{2J}/du^{2J} (black bar) mice at P21 ($n = 4$). All comparisons were made between littermates in ***A*** and ***B*** and in ***D*** and ***E***.

plemental Table 5, available at www.jneurosci.org as supplemental material). However, the expression of the voltage-gated Na^+ channel (Na_V) β2 subunit (*Scn2b*) mRNA was downregulated to 81.8 ± 3.7% ($n = 10$) in du^{2J}/du^{2J} cerebellum, although there was no change in the expression of $Na_V\beta 4$ (*Scn4b*), $Na_v1.1$, or $Na_v1.6$ (Fig. 5*D* and supplemental Table 5, available at www.jneurosci.org as supplemental material). In this regard, it is of interest that $Na_V\beta 2$ is one of the binding partners for tenascin-C (Srinivasan et al., 1998).

Expression of $\alpha_2\delta$-2 and tenascin-C protein in du^{2J}/du^{2J} cerebellum

We examined the presence of full-length $\alpha_2\delta$-2 protein in the cerebellum of the three genotypes (Fig. 6*A*). When proteins from $+/+$ cerebella are separated on SDS-PAGE under reducing conditions, free α_2-2 is detected with an anti-peptide Ab against amino acids 102–117 of $\alpha_2\delta$-2 (Fig. 6*A*). This protein was absent from du^{2J}/du^{2J} cerebellum and was consistently reduced by >50% in $du^{2J}/+$ cerebellum (Fig. 6*A*,*B*). We also examined whether the 40 kDa truncated protein that is potentially formed as a result of the presence of the 2 bp deletion in *Cacna2d2* could be detected in du^{2J}/du^{2J} cerebellum. A cDNA construct identical to this predicted product was made and expressed in Cos7 cells. It was detected with the α_2-2(102–117) Ab when expressed in Cos7 cells, but no equivalent endogenous product was present in du^{2J}/du^{2J} cerebellum (Fig. 6*C*). This is in agreement with the substantial reduction in $\alpha_2\delta$-2 mRNA in du^{2J}/du^{2J} cerebellum (supplemental Table 2, available at www.jneurosci.org as supplemental material), which is likely to be a result of nonsense-mediated message decay. However, the result is in contrast to the existence of a truncated α_2-2 protein in cerebellum from the original *du/du* strain, in which the truncation is attributable to a genetic rearrangement, rather than the presence of nonsense codons within the coding region (Brodbeck et al., 2002).

Tenascin-C is an extracellular matrix protein that is involved in normal neuronal development, synaptic plasticity, and angiogenesis (Meiners et al., 1999; Joester and Faissner, 2001; Evers et al., 2002). Because of the reduced expression of tenascin-C mRNA in du^{2J}/du^{2J} cerebellum at P21, we also examined the level of tenascin-C protein in du^{2J}/du^{2J} compared with WT cerebellum by Western blotting (Fig. 6*D*). Surprisingly, no alteration in the ~250 kDa tenascin-C protein was observed at P21 in du^{2J}/du^{2J} cerebellum (Fig. 6*D*,*E*), suggesting that the turnover of this extracellular matrix protein may be low. Tenascin-C exhibits several isoforms, and a progressive decrease in tenascin-C protein molecular weight has been reported to occur during cerebellar development (Bartsch et al., 1992). This was also observed in the present study, but no difference in the pattern of bands was observed between $+/+$ and du^{2J}/du^{2J} at earlier ages (P0 and P7; data not shown). Because tenascin-C binds to the exofacial domains of several $Na_V\beta$ subunits, we also examined whether tenascin-C might bind to $\alpha_2\delta$-2. Although certain *in vitro*-expressed domains of tenascin-C were able to pull down $\alpha_2\delta$-2, we were unable to coimmunoprecipitate endogenous $\alpha_2\delta$-2 and endogenous tenascin-C from cerebellum, so this remains an open question (I. Foucault and A. C. Dolphin, unpublished results).

Morphological changes in du^{2J}/du^{2J} cerebellum

The cerebella of du^{2J}/du^{2J} mice are smaller than their WT counterparts by about P15. In the original *du/du* allele, some PCs were observed to show abnormal dendrites, as well as axonal swellings that are indicative of degenerating neurons (Brodbeck et al., 2002). This could, in itself, cause changes to PC activity and so could have been a reason for ataxia. Calbindin was used as a marker of PCs, and its staining compared in P21 $+/+$ and du^{2J}/du^{2J} cerebellar sections (Fig. 7*A*). No major differences in cerebellar organization were observed in du^{2J}/du^{2J} sections, although there was a tendency for smaller and more closely packed PCs (Fig. 7*A*,*B*) and there was also evidence of axonal swelling in du^{2J}/du^{2J} sections observed at P21 ($n = 3$ mice) (Fig. 7*B*). Tenascin-C immunoreactivity was present in small cell bodies mainly concentrated in the PC layer, presumably Bergmann glia, and was also associated with blood vessels in cerebellar sections (data not shown), but no clear evidence of a difference between $+/+$ and du^{2J}/du^{2J} was observed. Furthermore, there was no evidence of microglial activation, which would be indicative of neurodegeneration in du^{2J}/du^{2J} cerebellum at P21 (V. H. Perry, M. Rees, and Dolphin, unpublished results). We also filled some PCs from which recordings were made with a fluorescent dye, Alexa-594, via the patch electrode. In du^{2J}/du^{2J} PCs, the dendrites appeared to be normal in terms of the extent of arborization of the primary dendrite (Fig. 8*A*,*B*), although the area occupied by the dendrites was smaller (Fig. 8*A*,*C*).

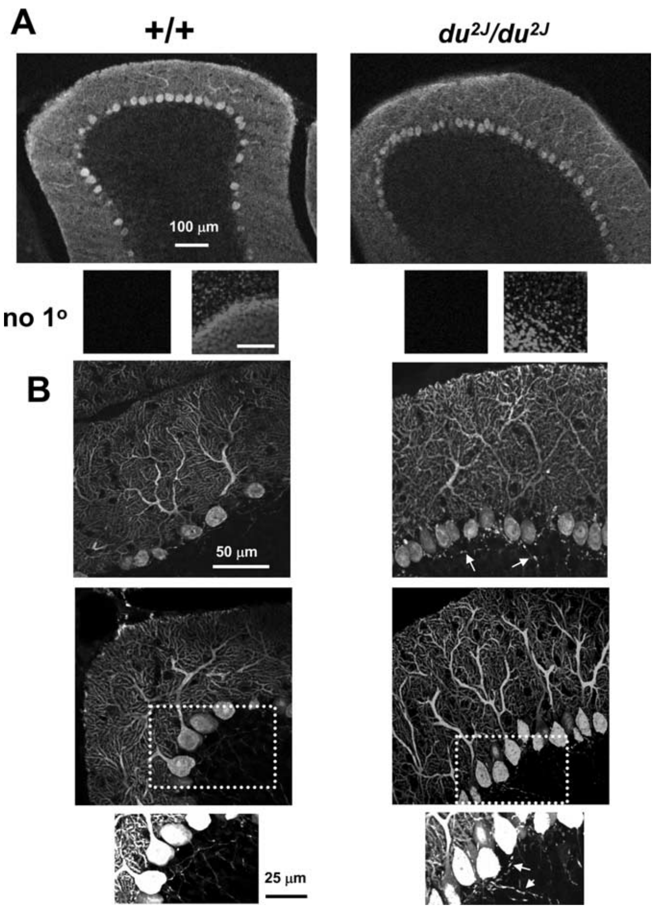

Figure 7. Immunohistochemistry for calbindin in sections from $+/+$ and *du^{2J}/du^{2J}* cerebellum. ***A***, Representative images taken from cerebellar sections at P21 stained for calbindin are shown for $+/+$ (left) and *du^{2J}/du^{2J}* (right). The objective (and optical section) used was 10× (13.7 μm). Beneath the sections, a negative control with no primary (1°) Ab (left), which was also stained with 4′,6-diamidino-2-phenylindole (right) to show their position at the border of the granule and molecular layers, is shown. Scale bar, 100 μm. ***B***, Representative projections of *Z*-stacks of 18–20 confocal images taken from cerebellar sections stained for calbindin are shown for $+/+$ (left) and *du^{2J}/du^{2J}* (right). The images were taken with a 40× objective (1 μm optical section). The bottom panel shows enlargements of the regions indicated by the dotted boxes, to illustrate increased staining of axons of *du^{2J}/du^{2J}* PCs, indicated by the arrows.

Discussion

This study was designed to shed light on the mechanisms whereby the loss of $\alpha_2\delta$-2 protein results in the phenotype of cerebellar ataxia in *du^{2J}/du^{2J}* mice. The main electrophysiological findings are that the I_{Ba} density in *du^{2J}/du^{2J}* PC somata at P7–P11 was reduced by ~30% compared with +/+ PCs, with no compensatory enhancement of L-type currents. Furthermore, in slices from P17–P25 cerebella, the spontaneous tonic firing rate of *du^{2J}/du^{2J}* PCs was markedly reduced at 22°C and abolished at 34°C. This was an intrinsic property of these cells, because it was observed in the presence of inhibitors of synaptic activity.

In whole-cell mode, the V_{rest} for *du^{2J}/du^{2J}* PCs was approximately −47 mV, which is sufficiently depolarized to cause depolarization block of Na_V channels (Swensen and Bean, 2003; Sausbier et al., 2004). However, when the membrane potential was hyperpolarized, depolarizing current pulses were able to elicit action potentials, although this required significantly larger current injection in *du^{2J}/du^{2J}* compared with +/+ PCs and showed increased spike frequency accommodation. A reduction in depolarization-induced PC firing has been observed previously in the tottering allele Rolling Nagoya (Mori et al., 2000).

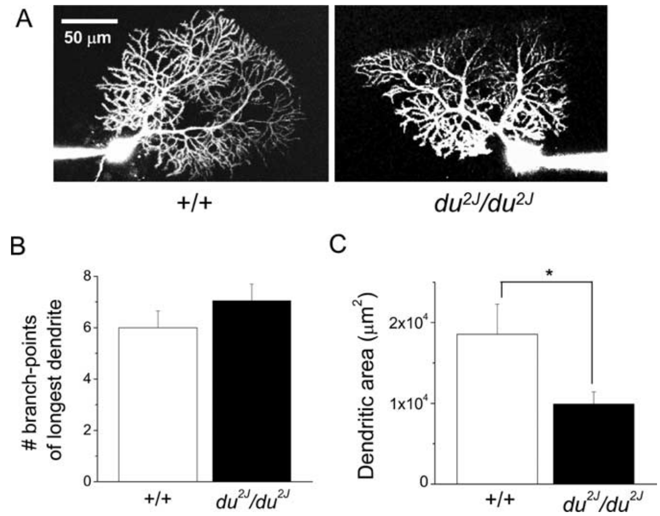

Figure 8. Morphology of cells filled with Alexa Fluor-594. ***A***, Examples of $+/+$ (left) and *du^{2J}/du^{2J}* (right) PCs filled with Alexa 594 during whole-cell recording. Scale bar, 50 μm. ***B***, Bar chart quantifying the number of branch points for the longest dendrite for $+/+$ ($n = 6$; □) and for *du^{2J}/du^{2J}* ($n = 5$; ■). ***C***, Bar chart showing the area occupied by the dendrites, quantified by forming a polygon of the dendritic tips, for $+/+$ ($n = 6$; □) and for *du^{2J}/du^{2J}* ($n = 6$; ■). $*p < 0.05$ (Student's nonpaired *t* test).

Mechanism of reduced firing rate of *du^{2J}/du^{2J}* PCs

Our results suggest that the inhibition of spontanous firing in *du^{2J}/du^{2J}* PCs was most likely attributable to depolarization block of Na_V channels as a result of the reduced activation of Ca^{2+}-dependent conductances. However, the phenotype of acute blockade of P-type channels with ω-agatoxin-IVB was not identical, because it resulted in an initial period of increased PC firing, followed by a complete cessation of firing.

Downstream of Ca^{2+} influx, it has been shown that activation of $I_{K(Ca)}$ plays an important role in the regulation of PC firing, and this is selectively activated by P-type calcium channels in these cells (Womack et al., 2004). However, spontaneous PC firing was not abolished by acute application of several $I_{K(Ca)}$ blockers, which increased the firing rate in +/+ PCs. Similar findings have been reported previously (Cingolani et al., 2002; Edgerton and Reinhart, 2003; Womack et al., 2004). Blockade of $I_{K(Ca)}$ increases firing frequency because of the reduced duration of the afterhyperpolarization, but this afterhyperpolarization also deinactivates Na_V channels, allowing subsequent action potential generation via the resurgent Na^+ current, thus regulating the frequency and regularity of repetitive firing (Swensen and Bean, 2003). These discrepancies indicate that there must be an additional involvement of other conductances or long-term compensatory changes that are involved in the reduction in firing frequency observed in *du^{2J}/du^{2J}* PCs.

It has been shown previously that deletion of the BK channel gene resulted in a similar ataxic phenotype to that observed in *du^{2J}/du^{2J}* mice, and this was also associated with a reduced spontaneous PC activity, which was attributed to depolarization block of Na_V channels (Sausbier et al., 2004). The authors noted that acute blockade of BK channels does not have the same phenotype as the BK channel knock-out, which is similar to our finding for *du^{2J}/du^{2J}* PCs. They also showed that the reduced spontaneous PC firing resulted in disinhibition of the deep cerebellar nuclei, to which the ataxic phenotype was attributed.

We have recently found that cerebellar $\alpha_2\delta$-2 and $Ca_V2.1$ are both strongly localized in lipid rafts (Davies et al., 2006), and it may be that this is relevant to their interaction with other ion channels, such as BK channels that have also been suggested to associate with lipid rafts (Bravo-Zehnder et al., 2000). It is also possible that $\alpha_2\delta$ subunits directly regulate other conductances and that this is involved in the mechanism of silencing in *du^{2J}/du^{2J}* PCs. Of interest in this regard, gabapentin (which binds to both $\alpha_2\delta$-1 and $\alpha_2\delta$-2 subunits) has been shown to enhance I_h (Surges et al., 2003), although it is unknown whether this occurs via $\alpha_2\delta$. Although I_h is known to regulate PC activity (Williams et al., 2002), we did not find differences in I_h between +/+ and *du^{2J}/du^{2J}* PCs.

Phenotype of *du^{2J}*/+ mice

We previously observed no phenotype in *du*/+ mice, in terms of obvious behavioral deficit or reduction in I_{Ba} in isolated PC somata (Barclay et al., 2001). *du^{2J}*/+ mice also show no overt behavioral phenotype. Furthermore, they have no reduction in somatic PC I_{Ba} at P7–P11 and no upregulation of cerebellar tyrosine hydroxylase mRNA at P21, in both of which they are identical to +/+ mice. However, *du^{2J}*/+ PCs do show an intermediate reduction in tonic spontaneous firing rate, although this is not accompanied by a significant decrease in regularity, as found in *du^{2J}/du^{2J}* PCs. However, the $\alpha_2\delta$-2 protein level is reduced by >50% in *du^{2J}*/+ cerebellum. It is therefore tempting to speculate that the partial reduction in $\alpha_2\delta$-2 in *du^{2J}*/+ cerebellum is responsible for the effect on PC firing frequency in *du^{2J}*/+ PCs, possibly by influencing extra-somatic calcium channel localization in relation to the other channels that maintain normal firing patterns, for example in the initial segment and first branchpoint of the axon, where both P-type calcium channels and Na_V channels show local concentrations (Callewaert et al., 1996; Clark et al., 2005). It is possible that calcium current density is reduced in intact *du^{2J}*/+ PCs and further depleted in *du^{2J}/du^{2J}* PCs in these extrasomatic regions, which would be lost in dissociated PC somata. This hypothesis will be addressed in future studies.

In contrast to our results, a recent study reported that there was no change in the predominant spontaneous firing frequency between *du/du*, *du*/+, and +/+ PCs, although a reduction in the regularity of firing was observed, with *du*/+ mice exhibiting an intermediate behavior, which could be normalized by application of an SK channel opener (Walter et al., 2006). Differences between our two studies include the fact that the original *du* mutation also involves duplication of a substantial region of chromosome 9 including the semaphorin-3B gene (Barclay et al., 2001). In addition, it results in the expression of a truncated protein from the *Cacna2d2* gene, which may have nonspecific effects (Brodbeck et al., 2002). Furthermore, the genetic background of *du/du* and *du^{2J}/du^{2J}* are different, and it is well established that this can affect observed channelopathy phenotypes (Sprunger et al., 1999). Other differences include the lower average age of the mice used in our study and our use of high-affinity rather than low-affinity excitatory amino acid antagonists to block excitatory synaptic activity.

Changes in gene expression in *du^{2J}/du^{2J}* cerebellum

Elevation of tyrosine hydroxylase gene expression in *du^{2J}/du^{2J}* cerebellum, which is also seen in some related cerebellar mutants (Hess and Wilson, 1991; Fureman et al., 1999; Sawada et al., 2001; Zwingman et al., 2001; Liu et al., 2003), points to aberrant intracellular Ca^{2+} regulation in *du^{2J}/du^{2J}* PCs (Nagamoto-Combs et al., 1997). Furthermore, the lack of elevation of tyrosine hydroxylase in *du^{2J}*/+ cerebellum correlates with the lack of reduction in their somatic PC calcium currents. Tyrosine hydroxylase protein is normally expressed transiently in PCs between P21 and P35, and is then downregulated (Hess and Wilson, 1991). In *tg/tg* mice, the continued elevation of cerebellar tyrosine hydroxylase was attributed to the entry of Ca^{2+} through L-type calcium channels, which show a compensatory increase in PCs of this mutant (Fureman et al., 1999). However, L-type calcium current was not elevated in *du^{2J}/du^{2J}* PC somata, and there was no increase in the expression of $Ca_V1.2$ mRNA in *du^{2J}/du^{2J}* cerebellum. Thus, the mechanism of elevation of expression of tyrosine hydroxylase remains unknown, as does its effect on PC function.

We found a marked reduction in tenascin-C mRNA in *du^{2J}/du^{2J}* cerebellum at P21. This suggests that there will be less *de novo* synthesis of tenascin-C. Certain $Na_V\beta$ subunits have been shown to interact extracellularly with tenascin-C (Srinivasan et al., 1998; Xiao et al., 1999). Thus, it is of interest that $Na_V\beta2$ mRNA is also significantly downregulated in *du^{2J}/du^{2J}* mice. *Scn2b* is mainly expressed by PCs in the cerebellum, and its interaction with tenascin-C may regulate the localization of Na^+ channels in PCs, in regions where they are important for the regulation of PC firing patterns, such as the axon initial segment. Both these results point to an altered distribution of Na_V channels in *du^{2J}/du^{2J}* PCs.

The role of $\alpha_2\delta$ subunits in the regulation of native Ca^{2+} currents

In many systems, $\alpha_2\delta$ subunits enhance heterologously expressed Ca^{2+} currents approximately threefold (Gurnett et al., 1996; Canti et al., 2003, 2005). However, the reduction in *du^{2J}/du^{2J}* PC I_{Ba} was only 30%, despite $\alpha_2\delta$-1 and $\alpha_2\delta$-3 showing little or no expression in PCs (Cole et al., 2005) and not being upregulated in *du/du* (Barclay et al., 2001) or *du^{2J}/du^{2J}* (present results) cerebellum. We have observed recently that expressed $\alpha_2\delta$-2 enhanced endogenous I_{Ba} in differentiated NG108-15 cells (Canti et al., 2005). Thus, there may be native calcium channels inserted into the plasma membrane, or competent to traffic to it, that do not have an associated $\alpha_2\delta$. In certain pathological situations, such as neuropathic pain, $\alpha_2\delta$ subunit expression is upregulated (Luo et al., 2001; Newton et al., 2001). It is likely that upregulation of $\alpha_2\delta$ subunits results in more funtional calcium channels, which may involve increased or differential trafficking or enhanced stability. Our study indicates that loss of $\alpha_2\delta$-2 has a profound effect on the function of PCs, in which it is the predominant species.

References

Barclay J, Balaguero N, Mione M, Ackerman SL, Letts VA, Brodbeck J, Canti C, Meir A, Page KM, Kusumi K, PerezReyes E, Lander ES, Frankel WN, Gardiner RM, Dolphin AC, Rees M (2001) Ducky mouse phenotype of epilepsy and ataxia is associated with mutations in the *Cacna2d2* gene and decreased calcium channel current in cerebellar Purkinje cells. J Neurosci 21:6095–6104.

Bartsch S, Bartsch U, Dorries U, Faissner A, Weller A, Ekblom P, Schachner M (1992) Expression of tenascin in the developing and adult cerebellar cortex. J Neurosci 12:736–749.

Bravo-Zehnder M, Orio P, Norambuena A, Wallner M, Meera P, Toro L, Latorre R, Gonzalez A (2000) Apical sorting of a voltage- and Ca2+-activated K+ channel alpha-subunit in Madin-Darby canine kidney cells is independent of N-glycosylation. Proc Natl Acad Sci USA 97:13114–13119.

Brill J, Klocke R, Paul D, Boison D, Gouder N, Klugbauer N, Hofmann F, Becker CM, Becker K (2004) entla, a novel epileptic and ataxic Cacna2d2 mutant of the mouse. J Biol Chem 279:7322–7330.

Brodbeck J, Davies A, Courtney J-M, Meir A, Balaguero N, Canti C, Moss FJ, Page KM, Pratt WS, Hunt SP, Barclay J, Rees M, Dolphin AC (2002) The ducky mutation in *Cacna2d2* results in altered Purkinje cell morphology and is associated with the expression of a truncated *a2d*-2 protein with abnormal function. J Biol Chem 277:7684–7693.

Burgess DL, Jones JM, Meisler MH, Noebels JL (1997) Mutation of the Ca2+ channel beta subunit gene Cchb4 is associated with ataxia and seizures in the lethargic (lh) mouse. Cell 88:385–392.

Callewaert G, Eilers J, Konnerth A (1996) Axonal calcium entry during fast 'sodium' action potentials in rat cerebellar Purkinje neurones. J Physiol (Lond) 495:641–647.

Campbell V, Berrow NS, Fitzgerald EM, Brickley K, Dolphin AC (1995) Inhibition of the interaction of G protein G_o with calcium channels by the calcium channel β-subunit in rat neurones. J Physiol (Lond) 485:365–372.

Canti C, Davies A, Dolphin AC (2003) Calcium channel alpha2delta subunits: structure, function and target site for drugs. Curr Neuropharmacol 1:209–217.

Canti C, Nieto-Rostro M, Foucault I, Heblich F, Wratten J, Richards MW, Hendrich J, Douglas L, Page KM, Davies A, Dolphin AC (2005) The metal-ion-dependent adhesion site in the Von Willebrand factor-A domain of alpha2delta subunits is key to trafficking voltage-gated Ca2+ channels. Proc Natl Acad Sci USA 102:11230–11235.

Chaudhuri D, Chang SY, DeMaria CD, Alvania RS, Soong TW, Yue DT (2004) Alternative splicing as a molecular switch for Ca^{2+}/calmodulin-dependent facilitation of P/Q-type Ca^{2+} channels. J Neurosci 24:6334–6342.

Chaudhuri D, Alseikhan BA, Chang SY, Soong TW, Yue DT (2005) Developmental activation of calmodulin-dependent facilitation of cerebellar P-type Ca^{2+} current. J Neurosci 25:8282–8294.

Cingolani LA, Gymnopoulos M, Boccaccio A, Stocker M, Pedarzani P (2002) Developmental regulation of small-conductance Ca^{2+}-activated K^+ channel expression and function in rat Purkinje neurons. J Neurosci 22:4456–4467.

Clark BA, Monsivais P, Branco T, London M, Hausser M (2005) The site of action potential initiation in cerebellar Purkinje neurons. Nat Neurosci 8:137–139.

Cole RL, Lechner SM, Williams ME, Prodanovich P, Bleicher L, Varney MA, Gu G (2005) Differential distribution of voltage-gated calcium channel alpha-2 delta (alpha2delta) subunit mRNA-containing cells in the rat central nervous system and the dorsal root ganglia. J Comp Neurol 491:246–269.

Crepel F (1971) Maturation of climbing fiber responses in the rat. Brain Res 35:272–276.

Davies A, Douglas L, Hendrich J, Wratten J, Tran Van Minh A, Foucault I, Koch D, Pratt WS, Saibil H, Dolphin AC (2006) The calcium channel $\alpha 2\delta$-2 subunit partitions with Cav2.1 into lipid rafts in cerebellum: implications for localization and function. J Neurosci 26:8748–8757.

Edgerton JR, Reinhart PH (2003) Distinct contributions of small and large conductance Ca2+-activated K+ channels to rat Purkinje neuron function. J Physiol (Lond) 548:53–69.

Evers MR, Salmen B, Bukalo O, Rollenhagen A, Bosl MR, Morellini F, Bartsch U, Dityatev A, Schachner M (2002) Impairment of L-type Ca^{2+} channel-dependent forms of hippocampal synaptic plasticity in mice deficient in the extracellular matrix glycoprotein tenascin-C. J Neurosci 22:7177–7194.

Fletcher CF, Lutz CM, O'Sullivan TN, Shaughnessy Jr JD, Hawkes R, Frankel WN, Copeland NG, Jenkins NA (1996) Absence epilepsy in tottering mutant mice is associated with calcium channel defects. Cell 87:607–617.

Fureman BE, Campbell DB, Hess EJ (1999) L-type calcium channel regulation of abnormal tyrosine hydroxylase expression in cerebella of tottering mice. Ann NY Acad Sci 868:217–219.

Gurnett CA, De Waard M, Campbell KP (1996) Dual function of the voltage-dependent Ca^{2+} channel $\alpha_2\delta$ subunit in current stimulation and subunit interaction. Neuron 16:431–440.

Hausser M, Clark BA (1997) Tonic synaptic inhibition modulates neuronal output pattern and spatiotemporal synaptic integration. Neuron 19:665–678.

Hess EJ, Wilson MC (1991) Tottering and leaner mutations perturb transient developmental expression of tyrosine hydroxylase in embryologically distinct Purkinje cells. Neuron 6:123–132.

Joester A, Faissner A (2001) The structure and function of tenascins in the nervous system. Matrix Biol 20:13–22.

Liu L, Zwingman TA, Fletcher CF (2003) In vivo analysis of voltage-dependent calcium channels. J Bioenerg Biomembr 35:671–685.

Luo ZD, Chaplan SR, Higuera ES, Sorkin LS, Stauderman KA, Williams ME, Yaksh TL (2001) Upregulation of dorsal root ganglion $\alpha_2\delta$ calcium channel subunit and its correlation with allodynia in spinal nerve-injured rats. J Neurosci 21:1868–1875.

Maquat LE (2002) Nonsense-mediated mRNA decay. Curr Biol 12:R196–R197.

Meier H (1968) The neuropathology of ducky, a neurological mutation of the mouse. A pathological and preliminary histochemical study. Acta Neuropathol Berl 11:15–28.

Meiners S, Mercado MLT, NureKamal MSA, Geller HM (1999) Tenascin-C contains domains that independently regulate neurite outgrowth and neurite guidance. J Neurosci 19:8443–8453.

Mori Y, Wakamori M, Oda S, Fletcher CF, Sekiguchi N, Mori E, Copeland NG, Jenkins NA, Matsushita K, Matsuyama Z, Imoto K (2000) Reduced voltage sensitivity of activation of P/Q-type Ca^{2+} channels is associated with the ataxic mouse mutation rolling Nagoya [tg(rol)]. J Neurosci 20:5654–5662.

Nagamoto-Combs K, Piech KM, Best JA, Sun B, Tank AW (1997) Tyrosine hydroxylase gene promoter activity is regulated by both cyclic AMP-responsive element and AP1 sites following calcium influx. Evidence for cyclic AMP-responsive element binding protein-independent regulation. J Biol Chem 272:6051–6058.

Newton RA, Bingham S, Case PC, Sanger GJ, Lawson SN (2001) Dorsal root ganglion neurons show increased expression of the calcium channel alpha2delta-1 subunit following partial sciatic nerve injury. Brain Res Mol Brain Res 95:1–8.

Page KM, Heblich F, Davies A, Butcher AJ, Leroy J, Bertaso F, Pratt WS, Dolphin AC (2004) Dominant-negative calcium channel suppression by truncated constructs involves a kinase implicated in the unfolded protein response. J Neurosci 24:5400–5409.

Sausbier M, Hu H, Arntz C, Feil S, Kamm S, Adelsberger H, Sausbier U, Sailer CA, Feil R, Hofmann F, Korth M, Shipston MJ, Knaus HG, Wolfer DP, Pedroarena CM, Storm JF, Ruth P (2004) Cerebellar ataxia and Purkinje cell dysfunction caused by Ca2+-activated K+ channel deficiency. Proc Natl Acad Sci USA 101:9474–9478.

Sawada K, Sakata-Haga H, Hisano S, Fukui Y (2001) Topological relationship between corticotropin-releasing factor- immunoreactive cerebellar afferents and tyrosine hydroxylase-immunoreactive Purkinje cells in a hereditary ataxic mutant, rolling mouse Nagoya. Neuroscience 102:925–935.

Snell GD (1955) Ducky, a new second chromosome mutation in the mouse. J Hered 46:27–29.

Sprunger LK, Escayg A, Tallaksen-Greene S, Albin RL, Meisler MH (1999) Dystonia associated with mutation of the neuronal sodium channel Scn8a and identification of the modifier locus Scnm1 on mouse chromosome 3. Hum Mol Genet 8:471–479.

Srinivasan J, Schachner M, Catterall WA (1998) Interaction of voltage-gated sodium channels with the extracellular matrix molecules tenascin-C and tenascin-R. Proc Natl Acad Sci USA 95:15753–15757.

Surges R, Freiman TM, Feuerstein TJ (2003) Gabapentin increases the hyperpolarization-activated cation current Ih in rat CA1 pyramidal cells. Epilepsia 44:150–156.

Swensen AM, Bean BP (2003) Ionic mechanisms of burst firing in dissociated Purkinje neurons. J Neurosci 23:9650–9663.

Walter JT, Alvina K, Womack MD, Chevez C, Khodakhah K (2006) Decreases in the precision of Purkinje cell pacemaking cause cerebellar dysfunction and ataxia. Nat Neurosci 9:389–397.

Williams SR, Christensen SR, Stuart GJ, Hausser M (2002) Membrane potential bistability is controlled by the hyperpolarization-activated current I(H) in rat cerebellar Purkinje neurons in vitro. J Physiol (Lond) 539:469–483.

Womack M, Khodakhah K (2002) Active contribution of dendrites to the tonic and trimodal patterns of activity in cerebellar Purkinje neurons. J Neurosci 22:10603–10612.

Womack MD, Chevez C, Khodakhah K (2004) Calcium-activated potassium channels are selectively coupled to P/Q-type calcium channels in cerebellar Purkinje neurons. J Neurosci 24:8818–8822.

Woodward D, Hoffer BJ, Lapham LW (1969) Postnatal development of electrical and enzyme histochemical activity in Purkinje cells. Exp Neurol 23:120–139.

Xiao ZC, Ragsdale DS, Malhotra JD, Mattei LN, Braun PE, Schachner M, Isom LL (1999) Tenascin-R is a functional modulator of sodium channel beta subunits. J Biol Chem 274:26511–26517.

Yamada K, Watanabe M (2002) Cytodifferentiation of Bergmann glia and its relationship with Purkinje cells. Anat Sci Int 77:94–108.

Zwingman TA, Neumann PE, Noebels JL, Herrup K (2001) Rocker is a new variant of the voltage-dependent calcium channel gene Cacna1a. J Neurosci 21:1169–1178.